Evaluating Dual-Frequency, Multi-Constellation GNSS Performance of Modern Smartphones for Atmospheric Monitoring Across Mountainous and Urban Areas

applied sciences

MDPI

Article

Novel Microfluidic Septum to Optimize Energy Recovery in Single-Chamber Microbial Fuel Cells

Giacomo Spisni [1,2,*], Giulia Massaglia [1,2], Valentina Bertana [1], Nicolò Vasile [2,3], Fabrizio C. Pirri [1,2], Stefano Bianco [1] and Marzia Quaglio [1,2,*]

[1] Department of Applied Science and Technology, Politecnico di Torino, 10129 Turin, Italy; giulia.massaglia@polito.it (G.M.); valentina.bertana@polito.it (V.B.); fabrizio.pirri@polito.it (F.C.P.); stefano.bianco@polito.it (S.B.)
[2] Istituto Italiano di Tecnologia, CSFT@PoliTo, 10144 Turin, Italy; nicolo.vasile@iit.it
[3] Department of Environment, Land and Infrastructure Engineering, Politecnico di Torino, 10129 Turin, Italy
* Correspondence: giacomo.spisni@iit.it (G.S.); marzia.quaglio@polito.it (M.Q.)

Abstract: This study proposes a redesign of asymmetric single-chamber microbial fuel cells (a-SCMFCs) with the goal of optimizing energy production. In the present work, the new approach is based on the introduction of a novel intermediate microfluidic septum (IMS) inside the electrolyte chamber. This IMS was designed as a relatively simple and inexpensive method to optimize both electrolyte flow and species transfer inside the devices. a-SCMFCs, featuring the IMS, are compared to control cells (IMS-less), when operated with sodium acetate as the carbon energy source. Performances of cells are evaluated in terms both of maximum output potential achieved, and energy recovery (E_{rec}) as the ratio between the energy yield and the inner electrolyte volume. The a-SCMFCs with the novel IMS are demonstrated to enhance the energy recovery compared to control cells exhibiting E_{rec} values of (37 ± 1) J/m^3, which is one order of magnitude higher than that achieved by control cells (3.0 ± 0.3) J/m^3. Concerning the maximum output potential, IMS cells achieve (2.8 ± 0.2) mV, compared to control cells at (0.68 ± 0.07) mV. Furthermore, by varying the sodium acetate concentration, the E_{rec} and maximum potential output values change accordingly. By monitoring the activity of a-SCMFCs for over one year, the beneficial impact of the IMS on both the initial inoculation phase and the long-term stability of electrical performance are observed. These improvements support the effectiveness of IMS to allow the development of efficient biofilms, likely due to the reduction in oxygen cross-over towards the anode. Electrochemical characterizations confirm that the presence of the IMS impacts the diffusion processes inside the electrolytic chamber, supporting the hypothesis of a beneficial effect on oxygen cross-over.

Keywords: microbial fuel cell; microfluidics; fluidic separator; single-chamber microbial fuel cell; energy recovery optimization

Citation: Spisni, G.; Massaglia, G.; Bertana, V.; Vasile, N.; Pirri, F.C.; Bianco, S.; Quaglio, M. Novel Microfluidic Septum to Optimize Energy Recovery in Single-Chamber Microbial Fuel Cells. *Appl. Sci.* **2023**, *13*, 11423. https://doi.org/10.3390/app132011423

Academic Editor: Dae Sung Lee

Received: 15 September 2023
Revised: 11 October 2023
Accepted: 16 October 2023
Published: 18 October 2023

1. Introduction

Concerns over climate change and energy security are pushing the demand for sustainable and reliable alternatives to fossil fuels. In this context, bio-electrochemical systems (BESs) represent a family of promising technologies for a wide range of applications, which include energy conversion into hydrogen by the so-called Microbial Electrolysis Cells (MECs) [1–3], microbial fuel cells (MFCs) for electrical power generation [4–6] and Microbial Electrosynthesis Cells for the valorization of CO_2 into new added-value products [7–9]. As an added benefit, BES operation can valorize the chemical energy entrapped in organic molecules present in wastewater, facilitating its remediation [5,10]. Among BESs, microbial fuel cells have drawn particular attention due to their ability to convert organic matter into electrical energy, leveraging the catalytic activity of the electroactive biofilm present at the anode electrode [4,6,11,12].

Notably, numerous studies are trying to address the issues currently associated with MFCs, among which are conversion efficiency, scalability, architecture, and cost-effectiveness [4,13–19]. Over the years, several MFC architectures have been investigated to enhance energy conversion and power production, with the possibility to be easily up-scalable [19]. MFC architectures can be classified into two main categories: two-compartment MFCs and single-compartment MFCs. The first category is characterized by an anodic and a cathodic chamber, usually separated by an ion-transporting membrane. The minimal design is represented by single-chamber MFCs (SCMFCs), which have shown significant potential in reducing the internal resistance of devices, simplifying fabrication, and reducing costs [20,21]. As discussed in the literature [22], the absence of an ion exchange membrane between the anodic and cathodic chambers ensures several advantages: it reduces mass transport limitation for species that are crucial for the metabolic activity of the anodic biofilm and entails a lower fabrication and maintenance complexity with respect to cells featuring membranes. At the same time, this may also represent a drawback as oxygen can more easily diffuse from the open-air cathode towards the bio-anode, negatively affecting its operation due to the proliferation of competing, non-electroactive microbes [4,22,23].

To this end, there is evidence in the literature of two main strategies to improve the overall membrane-less SCMFC. These are based on the reduction in oxygen cross-over in the proximity of anode electrodes, or the identification of the ideal distance between anode and cathode electrodes [24,25]. Another important feature, which directly affects the interaction between electrolyte and biofilm on the anode electrodes, was addressed by fluid dynamics studies [26–30]. Massaglia et al. [31,32] demonstrated that asymmetric a-SCMFCs, characterized by misaligned inlets and outlets, ensure a higher drift area, with an electrolyte flow characterized by a drop-like shape. The microfluidic-based design of a-SMFCs demonstrated an increase in the electrode surface area reached by the new electrolyte with each replacement. This led to confirmation that a drop-like shape configuration was suitable for the enhancement of the carbon-energy source distribution inside the devices, thus leading to an improvement in the overall a-SCMFCs' performance.

Analyzing the literature on single-chamber MFCs [24,25], an anode-to-cathode distance of 2 cm can represent an appropriate trade-off between maintaining good electrical performances while ensuring, in proximity of anodes' surfaces, a low amount of oxygen being dissolved in the electrolyte. This spacing can be achieved by the inclusion of a separating material, which also allows oxygen cross-over from the open-air cathode to be limited.

In the present work, we aimed at developing a new a-SCMFC configuration that conjugates the optimization of the electrolyte distribution under feeding conditions, by achieving an optimal drop-like shape, with the presence of a separator material suitable to minimize oxygen cross-over. As a solution, a modified a-SCMFC configuration by incorporating an intermediate microfluidic septum (IMS) was proposed. Such an IMS, without modifying the electrodes' spacing, occupies a significant portion of the internal cell's volume and features a pass-through opening. The primary intention behind the design of an IMS is to shape the reactor to exactly mimic the electrolyte flow patterns naturally occurring within the MFC during refills, so as to guarantee optimal electrolyte replenishment [31,32]. Moreover, compared to the usual square a-SCMFC design, the addition of the IMS in the cell's chamber reduces the amount of electrolyte required for this filling, but leaves the surface area of the electrodes unchanged. In addition, thanks to its shape, the IMS can act as a separator material to reduce the oxygen crossover near to the anode's surfaces, maintaining a distance between anode and cathode close to 1.8 cm, resulting in an adequate distance to minimize the amount of oxygen dissolved in the proximity of anode electrodes [26]. Furthermore, implementing the IMS configuration, this work demonstrates the tremendous impact of controlled fluid dynamics on the overall performance of a-SCMFCs. To give evidence of the crucial role of IMS configuration to improve the overall devices' performances, the energy recovery (E_{rec}) factor, defined as

the ratio between the output energy yield and the available electrolyte volume, has been analyzed [6,33–37]. The IMS design simultaneously addresses both aspects, improving energy output by optimizing biofilm electrical activity while also reducing the volume of the single-chamber electrolyte. Furthermore, a-SCMFCs with the IMS achieved an energy recovery one order of magnitude higher than that achieved by control cells, thus demonstrating the key role of microfluidics inside MFCs.

This study contributes to the advancement in MFC technology, providing an alternative solution that partly overcomes the disadvantages related to the absence of an ionic exchange membrane.

2. Materials and Methods

2.1. Design and Fabrication of a-SCMFCs

The structural components of the asymmetric, square, single-chamber MFCs, with open-air cathode configuration [31], were fabricated via 3D printing technology (Stratasys OBJET 30 with VeroWhite material). To ensure complete solvent removal, 3D-printed components were kept overnight in an oven at 110 °C. The a-SCMFCs were composed of three separate components kept together by screws and rubber sealing: an anodic compartment (air-tight), an intermediate spacing (with a window and inlet/outlet holes), and a (open-air) cathode compartment (Figure 1A,B). The available geometric area occupied by the electrodes in both the anode and cathode compartments was equal to 5.76 cm^2, and the inner volume occupied by the electrolyte was 12.5 mL.

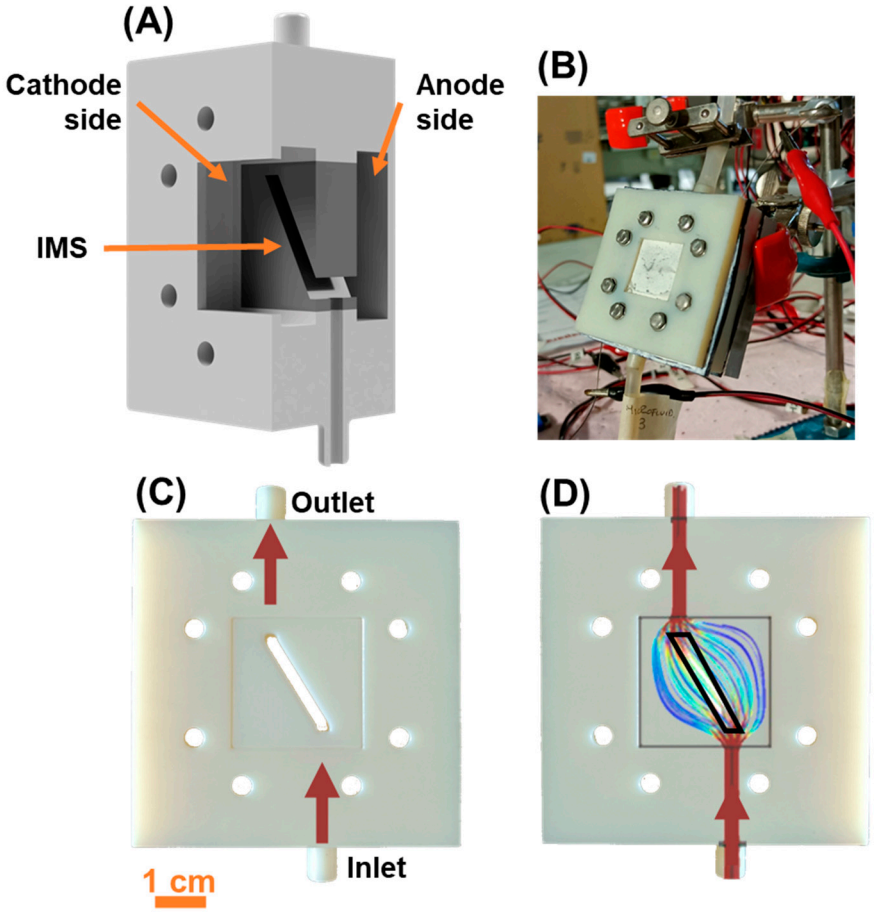

Figure 1. (**A**) Cross-sectional view of an a-SCMFC featuring the intermediate microfluidic septum proposed in this work. (**B**) Picture of an IMS cell connected to the experimental apparatus. (**C**) Intermediate spacing including the IMS proposed in this work. (**D**) Comparison with the flow field (without IMS) modeled in previous studies. The image of the flow field was adapted and re-printed with the permission of John Wiley and Sons from the article: [32].

The intermediate spacing component allowed us to perform cell refills through its top and bottom apertures. Moreover, the window present in such a spacing component permitted the insertion of the intermediate microfluidic septum (Figure 1A,C). The novel design of the IMS was based on knowledge acquired from previous studies [31,32] which modeled and studied the microfluidic flow field arising inside cells under normal operative conditions (Figure 1D). For the MFCs in this study, the IMS was designed to occupy the entire window present in the intermediate spacing, except for a narrow pass-through opening with a geometric area of 0.36 cm^2. With the IMS, the inner volume available for the electrolyte was reduced to 6.6 mL. The opening was oriented so as to connect both the inlet and outlet with a straight line, following the trajectory around which the flow field normally develops during electrolyte replenishment [31,32], as highlighted in Figure 1D.

To assess the contribution provided by the IMS, this experiment consisted of a triplet of cells featuring the IMS (here named IMS 1, IMS 2, and IMS 3) and a triplet of standard a-SCMFCs without the IMS as the controls (referred to as Control 1, Control 2, and Control 3). During the experiment, all IMS and control cells were simultaneously refilled using the same electrolyte solution.

As the anode, as-received carbon felt (FuelCell Store, Bryan, TX, USA) was used by cutting it into 30 × 30 mm^2 squares. Inside the cells, the anodes were held in place and electrically contacted by a 3D-printed frame threaded with titanium wire (Goodfellow Cambridge Limited, Huntingdon, UK). As the cathode electrode, a commercial AvCarb Gas Diffusion System (AvCarb Material Solutions, Lowell, MA, USA) was employed, composed of carbon paper, a poly-tetra-fluoro-ethylene (PTFE) treatment on the air-facing side, and micro-porous layer surface coating facing the electrolyte side. To promote the oxygen reduction reaction, a catalyst paste, to be spread on the cathodic micro-porous layer, was prepared according to previous works [38–40]. This paste was based on Platinum (10 wt% Pt on carbon, from Sigma Aldrich (St. Louis, MO, USA), final Pt loading 0.5 mg/cm^2) and Nafion (5 wt% Nafion, from Sigma Aldrich, final concentration 3 mg/cm^2), acting as a binder.

2.2. a-SCMFC Acclimation and Start-Up

The inoculation of the a-SCMFCs was performed with a mixed microbial consortium, obtained from the third enrichment of marine sediment (10% v/v; marine sediment was collected in La Spezia) [41,42]. Each enrichment was performed via dissolution into a water-based electrolyte, containing 12 mM of sodium acetate as the carbon energy source.

The acclimation phase for all a-SCMFCs was monitored for 15 days, evaluating the biofilm formation onto the anode surface, by implementing an external load of 470 Ω, which was shown to be suitable to induce the formation of biofilm [31,38]. After the acclimation phase, an external load of 1 kΩ was applied to directly evaluate the overall a-SCMFCs' performance. During this phase, named the start-up phase, the electrolyte solution was prepared via dissolution in de-ionized water sodium acetate with a concentration of 12 mM (1 g/L).

To ensure the optimal operation conditions, ammonium chloride (NH_4Cl, 0.31 g each, 1 g of sodium acetate) was added to provide a nitrogen source to aid microbial growth, potassium chloride (KCl, 0.13 g/L) as a mineral source, and sodium dihydrogen phosphate (NaH_2PO_4, 2.450 g/L) to maintain a stable neutral pH. All reagents were purchased from Sigma Aldrich, and the obtained electrolyte solutions were autoclaved prior to use.

The presence of an IMS leads to the achievement of the best performance compared to that achieved without the IMS. To demonstrate and confirm this consideration, we introduced a parameter called energy recovery, defined by the following Equation (1):

$$E_{rec} = \frac{\int_{t_1}^{t_2} P(t)dt}{V_{int}}, \quad (1)$$

where E_{rec} (J/m^3) is the energy recovery, V_{int} (m^3) is the internal volume of the MFCs, and $\int_{t_1}^{t_2} P(t)dt$ (J) is the integral of the recovered energy between the initial (t_1) and final (t_2) moments associated with each refill.

During the experiment, solutions with a reduced amount of sodium acetate were also tested. A different reduced concentration of sodium acetate with respect to the standard one (12 mM of sodium acetate) was proposed to confirm that the voltage output decreases as the concentration of sodium acetate decreases. Through this approach, it was intended to demonstrate the effectiveness of the IMS, which was shown to be suitable for the maximization of the response of IMS cells to changes in sodium acetate concentration. This hypothesis could be confirmed by the fact that the IMS ensured the distribution of fluid flow in a drop-like shape, thus leading to the maximization of the distribution of sodium acetate within the device and, therefore, improvements in the response of the IMS cells.

The analyzed concentrations were 8 mM (0.67 g/L), 4 mM (0.33 g/L), and 2 mM (0.17 g/L) During this part of the experiment, the composition of the electrolyte medium remained unchanged, except for the ammonium chloride concentration, which was reduced accordingly to preserve the same mass ratio as sodium acetate.

The a-SCMFCs were operated in fed-batch mode, with the electrolyte being replaced every 48 h to 72 h, in correspondence to which a voltage drop was observed. The fresh electrolyte was replaced when the voltage drop achieved a value close to 0 V.

2.3. Time Schedule of Experimental Activity

The experimental activity was subdivided into three phases.

1. The first phase coincided with the inoculation period, which allowed for the initial formation of the biofilm at the anode electrode [41,42]. During this first phase, the monitoring of the biofilm formation on the anode surface took place under a 470 Ω external load, which was shown to be suitable for the induction of the biofilm formation [31,38]. At the end of this phase, to directly evaluate the overall devices' performances, the external load was raised to 1 kΩ.
2. The second phase corresponded with a standard working period spanning over several months. This phase began with a start-up period, during which, a-SCMFCs transitioned to a standard 12 mM sodium acetate electrolyte medium. Throughout this working phase, it was possible to observe the stabilization of the a-SCMFCs' electrical output performance and assess how this varied over time.
3. The third phase consisted of a perturbation phase, during which, the concentration of sodium acetate dissolved in the electrolyte medium was systematically reduced. To this end, the electrical output performances of the IMS and control cells were compared while performing multiple refills at decreasing fixed concentrations of sodium acetate (12 mM, 8 mM, 4 mM, 2 mM), and then once again providing the standard concentration (12 mM) to verify the consistency of the results.

2.4. Electrical and Electrochemical Characterizations

During the experiment, the output potential of the a-SCMFCs was monitored by connecting each anode–cathode pair to a multichannel data acquisition unit (Keysight 34972A), controlled by a computer. All the experiments were conducted in triplicate, with cells kept at ambient temperature in a range of (20 ± 5) °C.

Throughout the experiment lifetime, Linear Sweep Voltammetry (LSV) and Electrochemical Impedance Spectroscopy (EIS) characterizations were performed to characterize electrical output performances and investigate the interfaces arising inside the cells at the anode electrode. All electrochemical characterizations were conducted using a PalmSens 4 (PalmSens BV, Houten, The Netherlands) potentiostat. For both LSV and EIS, a two-electrode configuration was employed, where the anode acted as a working electrode and the cathode as a counter and reference electrode. The EIS characterizations took place in an open-circuit condition by imposing an AC sinusoidal signal with 10 mV amplitude and frequency ranging from 200 mHz to 150 kHz. Afterwards, LSV measurements were

performed by sweeping, at a 0.1 V/s scan rate, the applied potential from its open-circuit value to a short circuit (0 V).

Both electrochemical characterizations, LSV and EIS, were implemented to evaluate the electrochemical performance of the anode electrode, which also allowed the electroactive behavior of microorganisms to be discriminated, correlating it with the presence or absence of an IMS inside the device.

3. Results

The following subsections describe the experimental results obtained while testing the a-SCMFC devices during the three phases of the experiment. Data obtained from the cells featuring the novel IMS are compared with reference a-SCMFCs without IMSs.

3.1. Inoculation Phase and Start-Up

During the inoculation period, proper biofilm growth on the anode electrode represents a crucial aspect in determining electrical output performance. The results obtained in this period allowed us to confirm that the presence of the IMS as a physical barrier allowed correct biofilm formation and, at the same time, ensured a shorter start-up time when compared with control cells.

Indeed, Figure 2 demonstrates how the output potential provided by the IMS was immediately comparable with that of the control cells, thus leading to confirmation of the correct proliferation of biofilm on the anode electrodes. Moreover, it was possible to appreciate that the IMS achieved reproducible voltage peaks within the first electrolyte replenishment. In comparison, control cells steadily reached the value of the first peak, but not until the third electrolyte replenishment (see Figure 2).

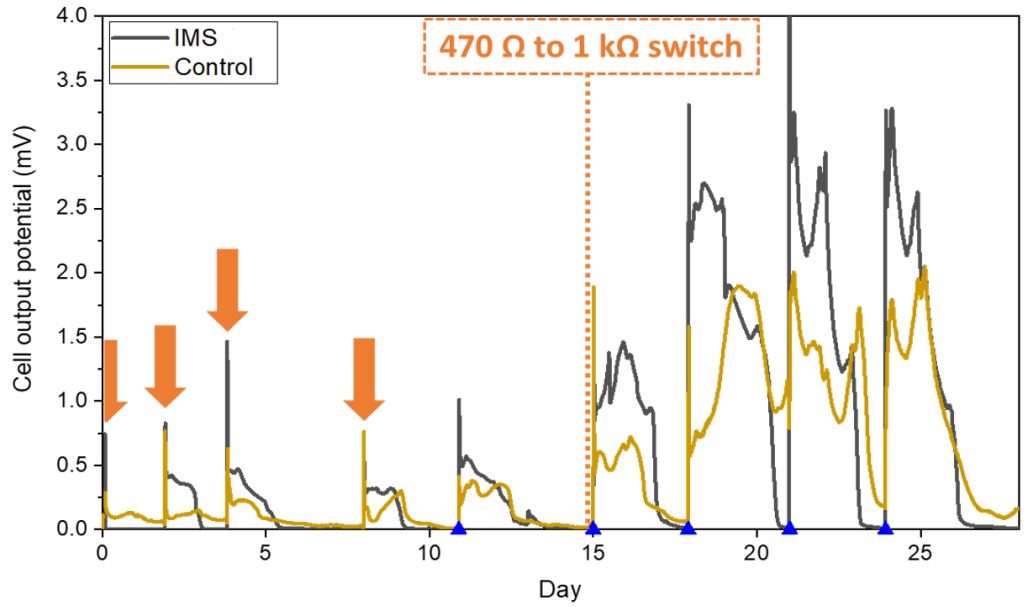

Figure 2. Cell output potential measured during the inoculation phase (from day 1 to day 15) and the beginning of the working phase (start-up period). Each arrow represents one electrolyte replenishment with inoculum medium, while triangles on the horizontal axis correspond to refills with 12 mM of sodium acetate electrolyte.

These results allowed us to demonstrate how, under normal operative conditions, the intermediate spacing resulted in being pivotal in ensuring proper electrolyte replenishment by developing the microfluidic flow field inside the cell. At the same time, such an IMS acted as a separator material, able to reduce oxygen crossover without modifying electrodes' spacing. Indeed, the electrodes' spacing was close to 1.8 cm, which, according to Cheng et al. [25], ensured an optimal reduction in the dissolved oxygen amount close to the anode surface for membrane-less SCMFCs. Moreover, these results were in line with

the hypothesis that optimizing the drop-shape electrolyte flow distribution by the IMS promotes biofilm formation by maximizing the interaction between the biofilm and the electrolyte [31,32].

Later, after raising the external load from 470 Ω to 1 kΩ, both the IMS and control cells reached a reproducible stable output within three refills (Figure 2). In conclusion, the presence of the IMS sped up the formation of a stable biofilm on the anode electrode, while also accelerating the acclimation process.

3.2. Working Phase on Standard Sodium Acetate Electrolyte

Following the initial inoculation phase and the start-up period, the cells operated for a period lasting over one year running on standard electrolytes with a 12 mM sodium acetate concentration. During this working period, the IMS cells presented peaks broadened in time with respect to the control cells (Figure 3A). To quantify this difference, for each refill event, how much time such output potential remained above the threshold set by the baseline potential was estimated, which corresponded to the minimum potential value close to 0.15 mV for IMS cells and 0.3 mV for control cells.

As outlined in Figure 3A, it was possible to appreciate the duration of peaks, which resulted in being (52 ± 5) hours for the IMS cells, and (36 ± 3) hours for the control cells. As later discussed in more detail, this prolonged electrical activity in IMS cells corresponded with a higher energy output compared to the control cells.

The evidence of prolonged electrical activity further suggested that the addition of the IMS likely favored optimal biofilm formation. Indeed, the presence of the IMS may have reduced oxygen cross-over towards the anode, promoting the acclimation of desirable electroactive microbial species, which are favored by anoxic conditions.

As the output potential of a-SCMFCs had been monitored for a prolonged period of time, it was possible to assess the long-term stability of their electrical output performances. Figure 3B allows us to compare the performance of IMS and control cells after two months and after one year of activity, thus leading us to state that IMS cells reached the maximum output potential of (2.8 ± 0.2) mV, which was one order of magnitude higher than that achieved by control cells, equal to (0.68 ± 0.07) mV. Moreover, from Figure 3B, it was possible to highlight how control cells experienced a higher decrease in electrical output performance compared to IMS cells. Thus, over time, the presence of the IMS provided steadier cell electrical activity.

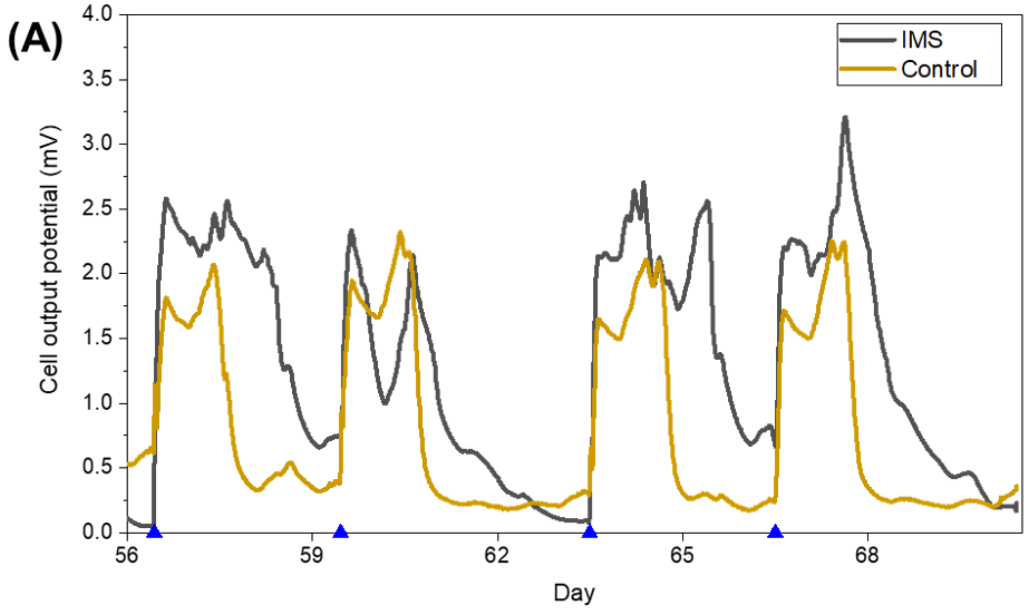

Figure 3. *Cont.*

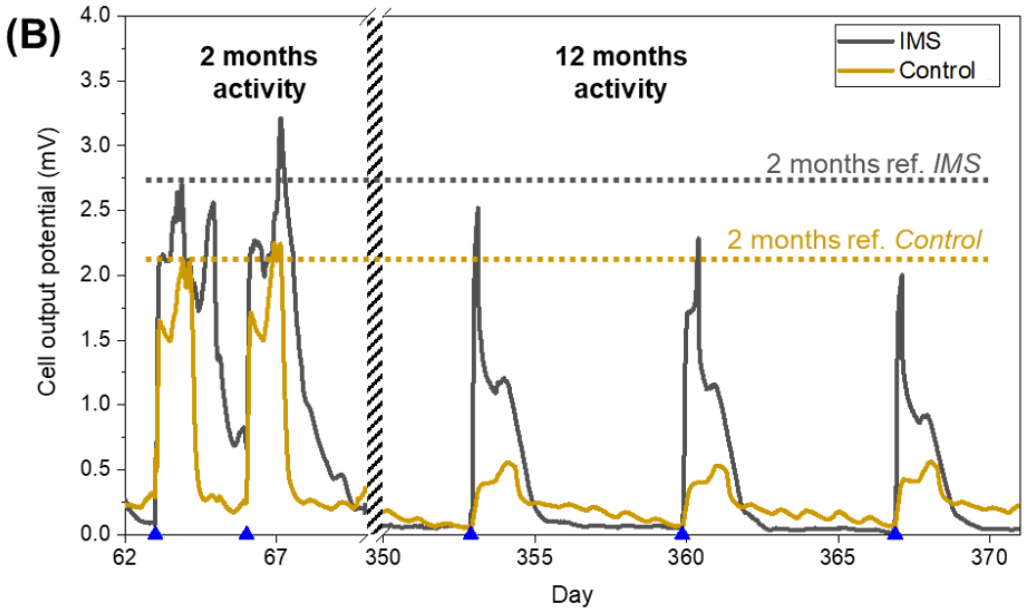

Figure 3. (**A**) Cell output potential measured after two months of activity during the standard working period. Each blue triangle represents one replenishment with electrolyte solution (12 mM sodium acetate concentration). It is possible to observe how the IMS cells provided peaks broadened in time compared to the control cells. (**B**) Comparison of cell output potential measured after two months (**left**) and one year (**right**) of activity. Each blue triangle represents one replenishment with standard electrolyte solution (12 mM sodium acetate concentration).

3.3. Perturbation Phase with Variable Sodium Acetate Concentration

As devices working in real scenarios rarely receive a controlled amount of carbon energy source, part of this work aimed to assess how cells featuring an IMS performed during periods of reduced nutrient availability. Since the overall devices' performances were strictly correlated with the metabolic activity of electroactive bacteria constituting the biofilm on the anode surface, it was possible to demonstrate the correlation between the maximum output potential generated by MFCs and the concentration of carbon energy source dissolved in the electrolyte [31,43]. To this end, over sets of consecutive refills, all the cells received electrolyte medium with sodium acetate molarity which reduced from 12 mM down to 2 mM. During this process, the composition of the electrolyte medium remained unchanged, except for the ammonium chloride concentration, which was reduced accordingly to preserve the same mass ratio as sodium acetate.

From the measured output potentials, it was possible to extract the maximum values reached by the cells after each refill. To reduce fluctuations associated with each cell, the measured maxima were averaged over each a-SCMFC triplet. Figure 4 represents the average peak maxima observed at different concentrations of sodium acetate in the electrolyte refill. It is possible to observe how the IMS cells systematically provided a higher output potential compared to the control cells. Indeed, at the standard 12 mM sodium acetate concentration, the IMS cells featured, on average, a maximum peak potential of (2.8 $\pm$ 0.2) mV, compared to the control cells at (0.68 $\pm$ 0.07) mV. Even at sodium acetate concentrations as low as 2 mM, the IMS cells provided average peak maxima at (0.60 $\pm$ 0.07) mV, higher than the control cells at (0.22 $\pm$ 0.02) mV.

Finally, it was possible to observe a cell's behavior when the sodium acetate concentration returned to 12 mM (empty-area symbols in Figure 4). In both cells, the observed trend was confirmed, by being able to return to output potentials compatible with the initial values of (2.7 $\pm$ 0.4) mV and (0.69 $\pm$ 0.08) mV for the IMS and control cells, respectively.

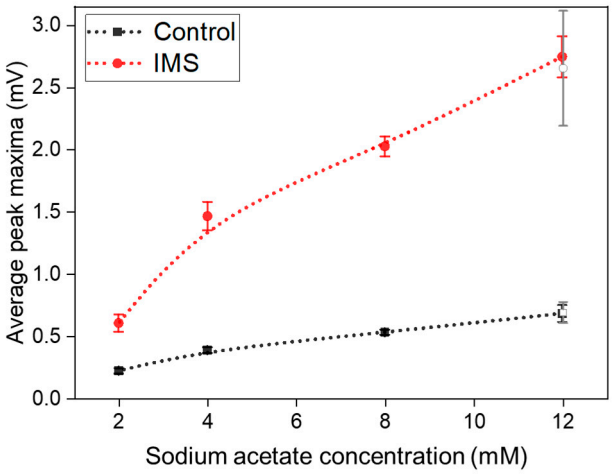

Figure 4. Average peak maxima as function of sodium acetate concentration (expressed in mM). The empty-area symbols correspond to peaks associated with 12 mM refills performed at the end of this perturbation phase, with the aim of validating the initial recorded response.

To fully assess the a-SCMFCs' performances, the energy recovery parameter previously defined in Equation (1) was also considered [6,33–37]. Thus, instead of only focusing on the maximum output potential of the MFC, the E_{rec} parameter considers the power output from the a-SCMFCs. Figure 5 represents the average energy recovery calculated at different concentrations of sodium acetate in the electrolyte refill. These average values were obtained by aggregating measurements from a-SCMFCs, as previously carried out for peak maxima analysis. Considering the standard 12 mM sodium acetate concentration, the IMS cells featured an average energy recovery of (37 ± 1) J/m^3, one order of magnitude higher than that reached by the control cells (3.0 ± 0.3) J/m^3. Also, for the minimum sodium acetate concentration (2 mM), the IMS cells outperformed the control cells, providing (0.8 ± 0.2) J/m^3 and (0.18 ± 0.03) J/m^3, respectively. It was then possible to verify how IMS cells provided higher E_{rec} compared to the control cells, thus providing an optimization of the a-SCFMC design.

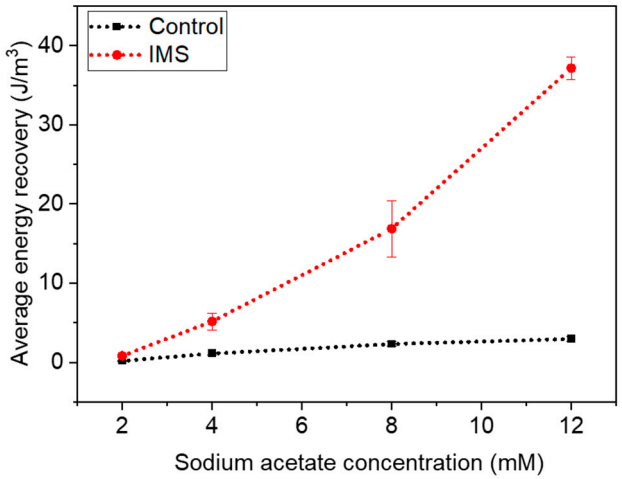

Figure 5. Average energy recovery as function of sodium acetate concentration (expressed in mM). IMS cells provided better electrical performances compared to control cells.

3.4. Electrochemical Characterizations

To assess in more detail the electrical performance of the a-SCMFCs, Linear Sweep Voltammetry (LSV) characterizations were performed. Figure 6 compares the polarization curves of one representative a-SCMFC from each triplet obtained after 8, 10, and 12 months

of activity. All current densities were calculated by normalizing the measured current to 5.76 cm^2, corresponding to the geometric area of the anode electrodes.

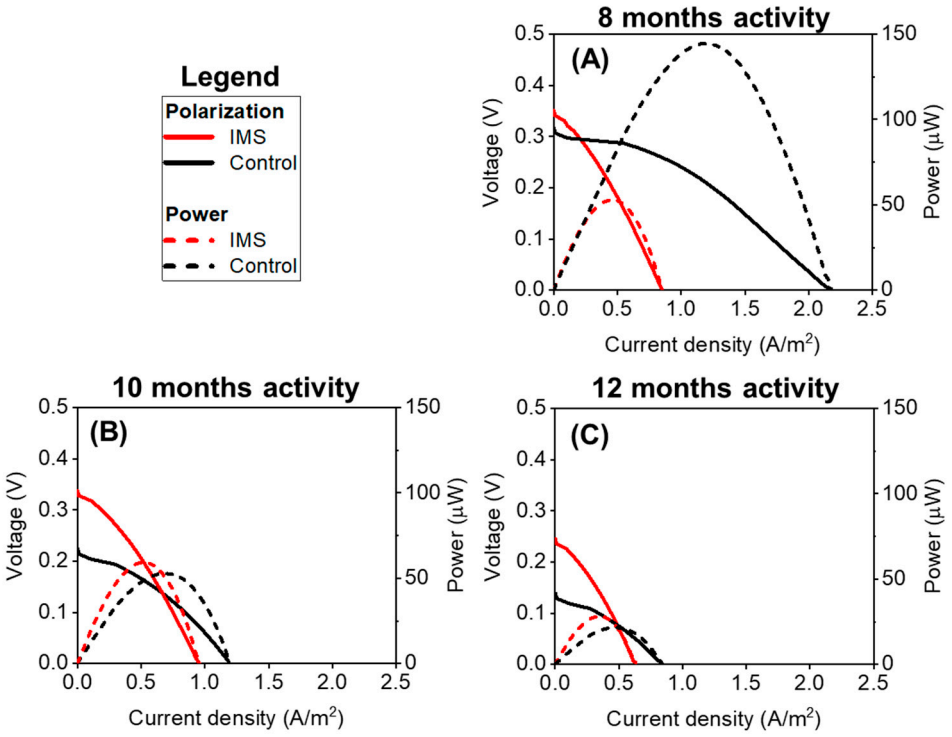

Figure 6. LSV analysis was performed on two representative cells at (**A**) 8 months, (**B**) 10 months, and (**C**) 12 months from the start of experimental activity. Red straight and dash lines represent IMS cells, while black straight and dash lines represent control cells. For both cells, solid lines represent the polarization curves (left vertical axis), while dashed lines correspond to the power curves (right vertical axis).

It is interesting to observe that the IMS cells provided a more stable response, in terms of smaller variations over time, compared to the control cells. This result agrees with what previously observed from output voltage monitoring (Figure 3B). In more detail, comparing Figure 6A–C, it was possible to appreciate that the open-circuit potential (OCP) for the IMS cells experienced less variability than the OCP for the control cells, which significantly decreased over time. A similar trend can be observed for the short-circuit currents. Finally, the linear region of the polarization curves allowed us to estimate an internal resistance of approximately 1 kΩ for the IMS cells and 500 Ω for the control cells.

Electrochemical Impedance Spectroscopy (EIS) was performed to gain a better understanding of the impedances associated with interfaces arising inside the a-SCMFCs. Based on the observed Nyquist plots, the impedance spectra could be modeled considering equivalent circuits previously described in the literature [44,45]. Figure 7 compares the Nyquist plots related to one representative a-SCMFC from each triplet. In particular, at the highest frequencies, it was possible to observe an ohmic (real) resistance representing impedances arising from electrodes, electrical contacts, and the electrolyte bulk. To focus on the features related to the electrochemical interfaces, plots were offset to suppress the contribution of this ohmic resistance.

As frequency decreased, the appearance of a distorted arc could be attributed to interfacial interactions at the electrode/microbial biofilm/electrolyte interface. Such impedance can be modeled as a parallel between its charge transfer resistance (R_{ct}) and a double-layer capacitance induced by the accumulation of charges. The distortion in the arc indicates a non-ideal capacitance behavior, likely due to the complex morphology and the porosity of electrodes [46,47]. In the equivalent circuit model, this corresponds to a constant-phase element. Focusing on this arc region of the Nyquist plot, over time, both the IMS and control

cells demonstrated a similar increase in charge transfer resistance. Specifically, the IMS cells experienced an R_{ct} increase from (17 ± 3) Ω (at 8 months) to (51 ± 6) Ω (at 17 months), and the control cells from (19.2 ± 0.6) Ω (at 8 months) to (46 ± 2) Ω (at 17 months). Finally, at lower frequencies, diffusion limitations became the dominant impedance contribution, and the presence of the IMS was more evident. Indeed, by acting as a physical barrier, the IMS introduced concentration losses that increased the overall measured impedance.

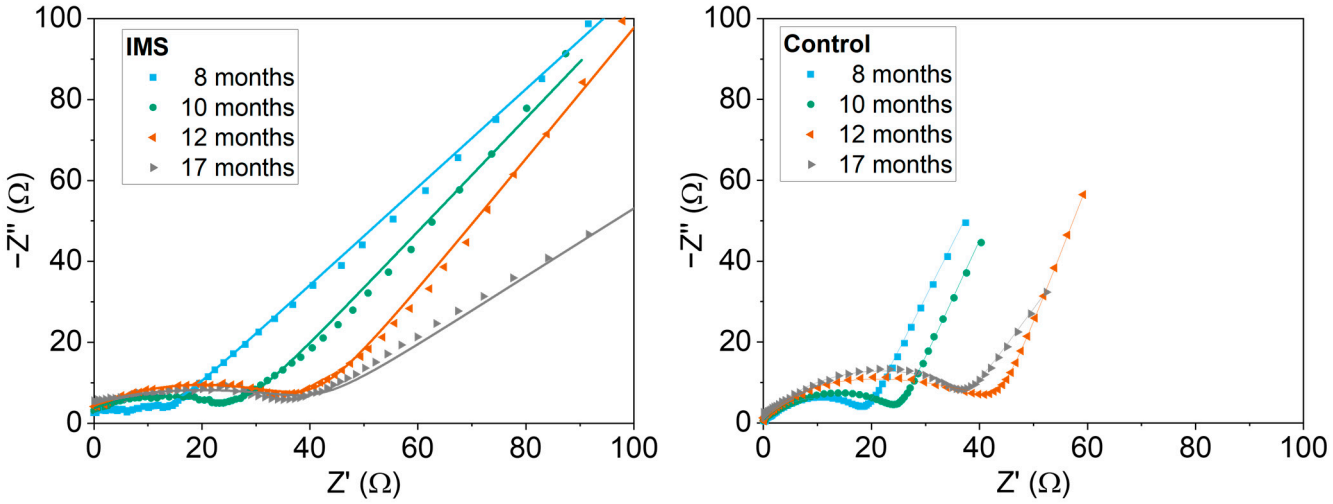

(**A**) (**B**)

Figure 7. EIS characterizations performed on two representative cells, (**A**) IMS and (**B**) control, throughout the experiment lifetime. Data acquired at 8, 10, and 12 months belong to the standard working phase, while the curve at 17 months corresponds with the conclusion of the perturbation phase.

4. Discussion

With the main purpose of enhancing the overall performance of asymmetric SCMFCs, this work proposes to optimize the electrolyte distribution by redesigning the inner volume of the reactors to give them a shape able to most effectively follow the spontaneous fluid flow field. The improved management of the electrolyte, ensured by the microfluidic septum, allows the energy conversion to be optimized, as demonstrated during all the phases, and as can be observed in Figures 2 and 3. Not only was the output voltage higher for the IMS cells, but the peaks were more stable and reproducible than the control cells. The improvement is further confirmed by the last phase of the experiment, during which, the carbon source concentration was changed over time. This result is particularly important since it shows that the IMS is able to optimize the inner environment of the cells in such a way to optimize the activity of the anodic biofilm. Indeed, the metabolic activity of electroactive bacteria is strictly correlated to the maximum output potential generated by MFCs and the concentration of the carbon energy source dissolved in the electrolyte [31,43].

These results show that, acting as a physical barrier interposed between the anode and the cathode, the IMS plays a crucial role in allowing for the optimization of the flow and then the cross-over of chemical species inside the reactor. Indeed, due to its aspect ratio shown in Figure 1A, the separator introduces mass transport limitations, also highlighted by Figure 7. One fundamental limitation is expected to involve oxygen: the IMS actually limits oxygen cross-over on the anode surface, thus minimizing the oxygen dissolved into the electrolyte in the proximity of biofilm growth onto anode electrodes. Nevertheless, the specific IMS design guarantees an appropriate electrolyte flow during cell refills and optimal replenishment with minimum perturbation of the internal environment. The experiments carried out in this study have clearly demonstrated that the beneficial effect of the biofilm protection against oxygen contamination is also the leading phenomenon, overcoming the barrier effect on other species, and thus ensuring better behavior than the control cells, especially for long-term applications, as shown in Figures 5 and 6. As

summarized in Table 1, it was possible to confirm the effective role of the IMS inside the a-SCMFCs, not only to mimic the drop-like shape typical of fluid flow distribution inside the devices, but also to minimize oxygen cross-over to the anode surface. Indeed, the presence of the IMS allowed good performances to be achieved in terms of voltage output and energy recovery. All these optimal results were obtained with IMS cells that presented an internal volume of 6.6 mL, which is lower than that reported in the literature. Also, fed-batch mode was implemented to refill the entire cells' volumes with fresh electrolytes. In addition, cells were fabricated without the introduction of ion exchange membranes and with a biofilm formed starting from a mixed consortium. All the underlined parameters and characteristics played a pivotal role in guaranteeing the potential future direct applicability of these devices in the environment.

Table 1. Literature references for comparison with different MFC designs.

MFC Designs	Performance Achieved	Ref.
• Dual-chamber MFC • Separator: Nafion 117 membrane • Internal volume: 50 mL • Sodium acetate concentration: 0.5 g/L	Maximum output voltage: 0.59 V, reached after 4 cycles.	[48]
• Air-cathode single-chamber MFC • Internal volume: 50 mL • Inoculum from aerobic activated sludge	Maximum open-circuit voltage: 791 mV.	[49]
• Miniaturized air-cathode single-chamber MFC • Two architectures: squared and drop-shaped • Sodium acetate variable concentration. The cells were operated in continuous mode	Maximum power density for both configurations was strictly correlated with the flow rate: the higher the flow rate, the higher the power density output. Drop-like architecture showed the largest power output.	[31]

5. Conclusions

In this work, the effective role of an intermediate microfluidic septum (IMS) in a-SCMFCs was demonstrated. Indeed, the IMS played a pivotal role in mimicking the fluid flow distribution according to a drop-like shape, thus ensuring a better distribution of sodium acetate close to the anode surfaces. All the obtained results, moreover, allowed us to confirm that the IMS could act as a separator material, able to minimize oxygen cross-over on anode electrodes and, consequently, to positively affect biofilm formation on the anodic electrodes. Indeed, during the start-up phase, the output potential provided by the IMS was immediately comparable with that of the control cells, thus leading us to confirm the correct proliferation of biofilm on the anode electrodes. Moreover, it was possible to appreciate that the IMS achieved reproducible voltage peaks within the first electrolyte replenishment. In comparison, the control cells steadily reached the value of the first peak, but not until the third electrolyte replenishment. Cells featuring an IMS had enhanced energy recovery from an electrolyte solution containing sodium acetate as the carbon energy source. By reducing the concentration of sodium acetate in the electrolyte medium, it was possible to verify that such overperformance persisted even when a smaller carbon energy source became available. In addition, in the long term, cells containing the IMS provided a more stable potential output compared to the control cells, suggesting that the development of the anodic biofilm might have been more efficient. All these optimal results were achieved with the proposed new configuration of an IMS cell that showed an internal volume of 6.6 mL, which is lower than that reported in the literature. Also, a fed-batch mode was implemented to refill the entire volume with fresh electrolytes; commercial carbon-based materials were employed as electrodes; and anodic biofilm was formed, starting from a mixed consortium. All these underlined parameters and characteristics played a pivotal role in guaranteeing the direct applicability of these devices in the environment.

Author Contributions: Conceptualization and methodology, M.Q., S.B., N.V. and G.M.; design and fabrication, V.B., G.S. and N.V.; experimental activity and data processing, G.S.; writing—original draft preparation, review and editing, G.S., G.M., M.Q. and S.B.; supervision and funding acquisition, F.C.P. All authors have read and agreed to the published version of the manuscript.

Funding: This research received no external funding.

Institutional Review Board Statement: Not applicable.

Informed Consent Statement: Not applicable.

Data Availability Statement: Data is unvailable.

Conflicts of Interest: The authors declare no conflict of interest.

References

1. Yang, E.; Omar Mohamed, H.; Park, S.-G.; Obaid, M.; Al-Qaradawi, S.Y.; Castaño, P.; Chon, K.; Chae, K.-J. A Review on Self-Sustainable Microbial Electrolysis Cells for Electro-Biohydrogen Production via Coupling with Carbon-Neutral Renewable Energy Technologies. *Bioresour. Technol.* **2021**, *320*, 124363. [CrossRef] [PubMed]
2. Escapa, A.; Mateos, R.; Martínez, E.J.; Blanes, J. Microbial Electrolysis Cells: An Emerging Technology for Wastewater Treatment and Energy Recovery. From Laboratory to Pilot Plant and Beyond. *Renew. Sustain. Energy Rev.* **2016**, *55*, 942–956. [CrossRef]
3. Lu, L.; Ren, Z.J. Microbial Electrolysis Cells for Waste Biorefinery: A State of the Art Review. *Bioresour. Technol.* **2016**, *215*, 254–264. [CrossRef] [PubMed]
4. Santoro, C.; Arbizzani, C.; Erable, B.; Ieropoulos, I. Microbial Fuel Cells: From Fundamentals to Applications. A Review. *J. Power Sources* **2017**, *356*, 225–244. [CrossRef] [PubMed]
5. Gude, V.G. Wastewater Treatment in Microbial Fuel Cells—An Overview. *J. Clean. Prod.* **2016**, *122*, 287–307. [CrossRef]
6. Logan, B.E. *Microbial Fuel Cells*; Wiley-Interscience: Hoboken, NJ, USA, 2008; ISBN 978-0-470-23948-3.
7. Dessì, P.; Rovira-Alsina, L.; Sánchez, C.; Dinesh, G.K.; Tong, W.; Chatterjee, P.; Tedesco, M.; Farràs, P.; Hamelers, H.M.V.; Puig, S. Microbial Electrosynthesis: Towards Sustainable Biorefineries for Production of Green Chemicals from CO_2 Emissions. *Biotechnol. Adv.* **2021**, *46*, 107675. [CrossRef]
8. Quraishi, M.; Wani, K.; Pandit, S.; Gupta, P.K.; Rai, A.K.; Lahiri, D.; Jadhav, D.A.; Ray, R.R.; Jung, S.P.; Thakur, V.K.; et al. Valorisation of CO_2 into Value-Added Products via Microbial Electrosynthesis (MES) and Electro-Fermentation Technology. *Fermentation* **2021**, *7*, 291. [CrossRef]
9. Rabaey, K.; Rozendal, R.A. Microbial Electrosynthesis—Revisiting the Electrical Route for Microbial Production. *Nat. Rev. Microbiol.* **2010**, *8*, 706–716. [CrossRef]
10. Kelly, P.T.; He, Z. Nutrients Removal and Recovery in Bioelectrochemical Systems: A Review. *Bioresour. Technol.* **2014**, *153*, 351–360. [CrossRef]
11. Aiyer, K.S. How Does Electron Transfer Occur in Microbial Fuel Cells? *World J. Microbiol. Biotechnol.* **2020**, *36*, 19. [CrossRef]
12. Prathiba, S.; Kumar, P.S.; Vo, D.-V.N. Recent Advancements in Microbial Fuel Cells: A Review on Its Electron Transfer Mechanisms, Microbial Community, Types of Substrates and Design for Bio-Electrochemical Treatment. *Chemosphere* **2022**, *286*, 131856. [CrossRef]
13. Priya, A.K.; Subha, C.; Kumar, P.S.; Suresh, R.; Rajendran, S.; Vasseghian, Y.; Soto-Moscoso, M. Advancements on Sustainable Microbial Fuel Cells and Their Future Prospects: A Review. *Environ. Res.* **2022**, *210*, 112930. [CrossRef] [PubMed]
14. Boas, J.V.; Oliveira, V.B.; Simões, M.; Pinto, A.M.F.R. Review on Microbial Fuel Cells Applications, Developments and Costs. *J. Environ. Manag.* **2022**, *307*, 114525. [CrossRef]
15. Palanisamy, G.; Jung, H.-Y.; Sadhasivam, T.; Kurkuri, M.D.; Kim, S.C.; Roh, S.-H. A Comprehensive Review on Microbial Fuel Cell Technologies: Processes, Utilization, and Advanced Developments in Electrodes and Membranes. *J. Clean. Prod.* **2019**, *221*, 598–621. [CrossRef]
16. Khan, M.E.; Khan, M.M.; Min, B.-K.; Cho, M.H. Microbial Fuel Cell Assisted Band Gap Narrowed TiO_2 for Visible Light-Induced Photocatalytic Activities and Power Generation. *Sci. Rep.* **2018**, *8*, 1723. [CrossRef] [PubMed]
17. Mohammad, A.; Karim, M.R.; Khan, M.E.; AlSukaibi, A.K.D.; Yoon, T. Eco-Benign Fabrication of Silver Nanoparticle-Modified Zeolitic Imidazolate Framework and Construction of a Non-Enzymatic Electrochemical Sensor. *Mater. Today Sustain.* **2022**, *19*, 100182. [CrossRef]
18. Mohammad, A.; Karim, M.R.; Khan, M.E.; Khan, M.M.; Cho, M.H. Biofilm-Assisted Fabrication of Ag@SnO_2-*g*-C_3N_4 Nanostructures for Visible Light-Induced Photocatalysis and Photoelectrochemical Performance. *J. Phys. Chem. C* **2019**, *123*, 20936–20948. [CrossRef]
19. Mathuriya, A.S.; Jadhav, D.A.; Ghangrekar, M.M. Architectural Adaptations of Microbial Fuel Cells. *Appl. Microbiol. Biotechnol.* **2018**, *102*, 9419–9432. [CrossRef]
20. Tamboli, E.; Eswari, J.S. Microbial Fuel Cell Configurations. In *Microbial Electrochemical Technology*; Elsevier: Amsterdam, The Netherlands, 2019; pp. 407–435, ISBN 978-0-444-64052-9.

21. Rossi, R.; Logan, B.E. Impact of Reactor Configuration on Pilot-Scale Microbial Fuel Cell Performance. *Water Res.* **2022**, *225*, 119179. [CrossRef]
22. Leong, J.X.; Daud, W.R.W.; Ghasemi, M.; Liew, K.B.; Ismail, M. Ion Exchange Membranes as Separators in Microbial Fuel Cells for Bioenergy Conversion: A Comprehensive Review. *Renew. Sustain. Energy Rev.* **2013**, *28*, 575–587. [CrossRef]
23. Chae, K.-J.; Choi, M.-J.; Kim, K.-Y.; Ajayi, F.F.; Chang, I.-S.; Kim, I.S. Selective Inhibition of Methanogens for the Improvement of Biohydrogen Production in Microbial Electrolysis Cells. *Int. J. Hydrogen Energy* **2010**, *35*, 13379–13386. [CrossRef]
24. Fan, Y.; Han, S.-K.; Liu, H. Improved Performance of CEA Microbial Fuel Cells with Increased Reactor Size. *Energy Environ. Sci.* **2012**, *5*, 8273. [CrossRef]
25. Cheng, S.; Liu, H.; Logan, B.E. Increased Power Generation in a Continuous Flow MFC with Advective Flow through the Porous Anode and Reduced Electrode Spacing. *Environ. Sci. Technol.* **2006**, *40*, 2426–2432. [CrossRef]
26. Kim, J.; Kim, H.; Kim, B.; Yu, J. Computational Fluid Dynamics Analysis in Microbial Fuel Cells with Different Anode Configurations. *Water Sci. Technol.* **2014**, *69*, 1447–1452. [CrossRef] [PubMed]
27. Zhao, L.; Li, J.; Battaglia, F.; He, Z. Investigation of Multiphysics in Tubular Microbial Fuel Cells by Coupled Computational Fluid Dynamics with Multi-Order Butler–Volmer Reactions. *Chem. Eng. J.* **2016**, *296*, 377–385. [CrossRef]
28. Kim, J.R.; Boghani, H.C.; Amini, N.; Aguey-Zinsou, K.-F.; Michie, I.; Dinsdale, R.M.; Guwy, A.J.; Guo, Z.X.; Premier, G.C. Porous Anodes with Helical Flow Pathways in Bioelectrochemical Systems: The Effects of Fluid Dynamics and Operating Regimes. *J. Power Sources* **2012**, *213*, 382–390. [CrossRef]
29. Sangeetha, T.; Li, I.-T.; Lan, T.-H.; Wang, C.-T.; Yan, W.-M. A Fluid Dynamics Perspective on the Flow Dependent Performance of Honey Comb Microbial Fuel Cells. *Energy* **2021**, *214*, 118928. [CrossRef]
30. Sobieszuk, P.; Zamojska-Jaroszewicz, A.; Makowski, Ł. Influence of the Operational Parameters on Bioelectricity Generation in Continuous Microbial Fuel Cell, Experimental and Computational Fluid Dynamics Modelling. *J. Power Sources* **2017**, *371*, 178–187. [CrossRef]
31. Quaglio, M.; Massaglia, G.; Vasile, N.; Margaria, V.; Chiodoni, A.; Salvador, G.P.; Marasso, S.L.; Cocuzza, M.; Saracco, G.; Pirri, F.C. A Fluid Dynamics Perspective on Material Selection in Microbial Fuel Cell-Based Biosensors. *Int. J. Hydrogen Energy* **2019**, *44*, 4533–4542. [CrossRef]
32. Massaglia, G.; Gerosa, M.; Agostino, V.; Cingolani, A.; Sacco, A.; Saracco, G.; Margaria, V.; Quaglio, M. Fluid Dynamic Modeling for Microbial Fuel Cell Based Biosensor Optimization. *Fuel Cells* **2017**, *17*, 627–634. [CrossRef]
33. Penteado, E.D.; Fernandez-Marchante, C.M.; Zaiat, M.; Cañizares, P.; Gonzalez, E.R.; Rodrigo, M.A. Energy Recovery from Winery Wastewater Using a Dual Chamber Microbial Fuel Cell. *J. Chem. Technol. Biotechnol.* **2016**, *91*, 1802–1808. [CrossRef]
34. Yang, G.; Wang, J.; Zhang, H.; Jia, H.; Zhang, Y.; Cui, Z.; Gao, F. Maximizing Energy Recovery from Homeostasis in Microbial Fuel Cell by Synergistic Conversion of Short-Chain Volatile Fatty Acid. *Bioresour. Technol. Rep.* **2019**, *7*, 100200. [CrossRef]
35. Capodaglio, A.G.; Molognoni, D.; Dallago, E.; Liberale, A.; Cella, R.; Longoni, P.; Pantaleoni, L. Microbial Fuel Cells for Direct Electrical Energy Recovery from Urban Wastewaters. *Sci. World J.* **2013**, *2013*, 634738. [CrossRef] [PubMed]
36. Massaglia, G.; Frascella, F.; Chiadò, A.; Sacco, A.; Marasso, S.L.; Cocuzza, M.; Pirri, C.F.; Quaglio, M. Electrospun Nanofibers: From Food to Energy by Engineered Electrodes in Microbial Fuel Cells. *Nanomaterials* **2020**, *10*, 523. [CrossRef] [PubMed]
37. Bird, H.; Heidrich, E.S.; Leicester, D.D.; Theodosiou, P. Pilot-Scale Microbial Fuel Cells (MFCs): A Meta-Analysis Study to Inform Full-Scale Design Principles for Optimum Wastewater Treatment. *J. Clean. Prod.* **2022**, *346*, 131227. [CrossRef]
38. Cheng, S.; Liu, H.; Logan, B.E. Power Densities Using Different Cathode Catalysts (Pt and CoTMPP) and Polymer Binders (Nafion and PTFE) in Single Chamber Microbial Fuel Cells. *Environ. Sci. Technol.* **2006**, *40*, 364–369. [CrossRef] [PubMed]
39. Massaglia, G.; Margaria, V.; Fiorentin, M.R.; Pasha, K.; Sacco, A.; Castellino, M.; Chiodoni, A.; Bianco, S.; Pirri, F.C.; Quaglio, M. Nonwoven Mats of N-Doped Carbon Nanofibers as High-Performing Anodes in Microbial Fuel Cells. *Mater. Today Energy* **2020**, *16*, 100385. [CrossRef]
40. Rossi, R.; Logan, B.E. Impact of External Resistance Acclimation on Charge Transfer and Diffusion Resistance in Bench-Scale Microbial Fuel Cells. *Bioresour. Technol.* **2020**, *318*, 123921. [CrossRef]
41. Massaglia, G.; Margaria, V.; Sacco, A.; Tommasi, T.; Pentassuglia, S.; Ahmed, D.; Mo, R.; Pirri, C.F.; Quaglio, M. In Situ Continuous Current Production from Marine Floating Microbial Fuel Cells. *Appl. Energy* **2018**, *230*, 78–85. [CrossRef]
42. Tommasi, T.; Salvador, G.P.; Quaglio, M. New Insights in Microbial Fuel Cells: Novel Solid Phase Anolyte. *Sci. Rep.* **2016**, *6*, 29091. [CrossRef]
43. Spurr, M.W.A.; Yu, E.H.; Scott, K.; Head, I.M. Extending the Dynamic Range of Biochemical Oxygen Demand Sensing with Multi-Stage Microbial Fuel Cells. *Environ. Sci. Water Res. Technol.* **2018**, *4*, 2029–2040. [CrossRef]
44. Wang, H.; Long, X.; Sun, Y.; Wang, D.; Wang, Z.; Meng, H.; Jiang, C.; Dong, W.; Lu, N. Electrochemical Impedance Spectroscopy Applied to Microbial Fuel Cells: A Review. *Front. Microbiol.* **2022**, *13*, 973501. [CrossRef] [PubMed]
45. Agostino, V.; Ahmed, D.; Sacco, A.; Margaria, V.; Armato, C.; Quaglio, M. Electrochemical Analysis of Microbial Fuel Cells Based on Enriched Biofilm Communities from Freshwater Sediment. *Electrochimica Acta* **2017**, *237*, 133–143. [CrossRef]
46. Park, S.-G.; Rhee, C.; Jadhav, D.A.; Eisa, T.; Al-Mayyahi, R.B.; Shin, S.G.; Abdelkareem, M.A.; Chae, K.-J. Tailoring a Highly Conductive and Super-Hydrophilic Electrode for Biocatalytic Performance of Microbial Electrolysis Cells. *Sci. Total Environ.* **2023**, *856*, 159105. [CrossRef] [PubMed]

47. Hidalgo, D.; Sacco, A.; Hernández, S.; Tommasi, T. Electrochemical and Impedance Characterization of Microbial Fuel Cells Based on 2D and 3D Anodic Electrodes Working with Seawater Microorganisms under Continuous Operation. *Bioresour. Technol.* **2015**, *195*, 139–146. [CrossRef]
48. Qiu, S.; Wang, L.; Zhang, Y.; Yu, Y. Microbial Fuel Cell-Based Biosensor for Simultaneous Test of Sodium Acetate and Glucose in a Mixed Solution. *Int. J. Environ. Res. Public Health* **2022**, *19*, 12297. [CrossRef] [PubMed]
49. Khater, D.Z.; El-Khatib, K.M.; Hassan, H.M. Microbial Diversity Structure in Acetate Single Chamber Microbial Fuel Cell for Electricity Generation. *J. Genet. Eng. Biotechnol.* **2017**, *15*, 127–137. [CrossRef]